Available online at www.sciencedirect.com
ScienceDirect
Journal of Power Sources 159 (2006) 478–483
JOURNAL OF POWER SOURCES
www.elsevier.com/locate/jpowsour

Fabrication and performance evaluation of 3-cell SOFC stack based on planar 10 cm × 10 cm anode-supported cells

H.Y. Jung, S.-H. Choi, H. Kim, J.-W. Son, J. Kim, H.-W. Lee, J.-H. Lee *

Nano-Materials Research Center, Korea Institute of Science and Technology, 39-1 Hawolgok-dong, Seongbuk-gu, Seoul 136-791, Republic of Korea

Received 22 June 2005; accepted 21 October 2005
Available online 20 December 2005

Abstract

This study reports the development of planar-type solid oxide fuel cell (SOFC) stacks based on an internal gas manifold and a cross-flow type design. A single-columned, 3-cell, SOFC stack is assembled using 10 cm × 10 cm anode-supported unit cells, metallic interconnects and glass-based compression-seal gaskets. The power-generating characteristics of the unit cell and stack are characterized as a function of temperature. The practical viability of the stack and stack components is investigated via long-term operation and thermal cycling tests. According to performance evaluation at 700 °C, the short stack produces about 100 W in total power at an average cell voltage of around 0.7 V. There are, however, some scale-up problems related to multi-cell stacking. This work addresses key issues in stack fabrication and performance improvement.

Keywords: Solid oxide fuel cell; Stack performance; Anode-supported cell; Interconnect; Sealing gasket; Scale-up problems

1. Introduction

The solid oxide fuel cell (SOFC) has been developed for next-generation power systems, which combine heat and electrical power. Recently, the SOFC has received more attention, due to its high efficiency, high waste-heat utilization and high fuel flexibility—all of which are the major motives behind replacing the conventional combination of a central power station and decentralized domestic heating systems. Nonetheless, SOFC still has a number of drawbacks in its application to an actual power system. Above all, the reliability and cost competitiveness of the SOFC system are recognized as the key technical barriers that hinder the entry of SOFCs into commercial market. Therefore, most research and development activities on SOFCs are focused mainly on the development of commercially-viable SOFC technology with high electrochemical performance and long-term stability [1–3].

There are two basic designs of planar-type SOFCs: electrolyte-supported and electrode-supported [1]. The electrolyte-supported SOFC has a rather simple fabrication procedure. On the other hand, the higher ohmic resistance due to the thick electrolytes (about 150–200 μm) requires a high operating temperature of around 1000 °C. Although this is somewhat favourable for a heat and power co-generation system, high temperature normally has seriously adverse effects on the stability and reliability of a cell stack, due to degradation of the constituent materials and components over a long operation time. Therefore, the current focal point of research and development to enhance SOFC performance is to reduce the operating temperature to a level at which reliability and cost competitiveness can be guaranteed.

In our previous studies [4,5], we have successfully fabricated high-performance, anode-supported, 5 cm × 5 cm unit cells with optimized electrode microstructures. In particular, a novel current-collecting layer was successfully constructed on the cathode and its current-collecting capability was verified during unit cell operation. By using the optimized cathode and current-collecting layer, three improvements were obtained simultaneously: (i) a decrease in overall ohmic resistance, especially the contact resistance; (ii) an improvement in the charge transfer due to a more interconnected structure of the cathode; (iii) an improvement in the mass transfer of dissolved oxygen, as the pores are distributed rather uniformly over the entire cathode structure [6]. As a result, a current-collecting layer with a con-

* Corresponding author. Tel.: +82 29585532; fax: +82 29585529.
E-mail address: jongho@kist.re.kr (J.-H. Lee).

0378-7753/$ – see front matter © 2005 Elsevier B.V. All rights reserved.
doi:10.1016/j.jpowsour.2005.10.103

trolled microstructure can enhance the unit cell performance by reducing the ohmic and/or polarization resistance of the cathode.

Based on the above findings, a larger sized (10 cm × 10 cm), anode-supported, unit cell with an improved cathode has been fabricated and applied to the manufacture of short SOFC stacks. This paper, discusses the development of SOFC stacks based on these anode-supported unit cells as a plausible means to achieve low or intermediate operating temperatures of around 700–750 °C. The fabrication procedure of the planar-type stack and its performance are reported. The key issues in fabricating the stack and the stack components are addressed with respect to higher performance and long-term reliability.

2. Experimental

In our previous investigations [4,5], high-performance anode-supported SOFCs were developed for operation at intermediate temperatures (700–800 °C). Fine yttria-stabilized zirconia (Tosoh, Japan), coarse yttria-stabilized zirconia (YSZ, Unitec, USA) and nickel oxide (J.T. Baker, USA) powders were used to prepare the NiO/YSZ anode substrate. The granulated NiO/YSZ composite powders were compacted by means of uni-axial pressing into a green anode substrate. An anode functional layer, which had the same composition as the anode substrate while containing only fine YSZ powder, was deposited on NiO/YSZ substrate via screen-printing. A very thin (less than 10 μm) YSZ electrolyte layer was also screen-printed on to the anode functional layer and co-fired at 1400 °C in air for 3 h.

The raw powders of $(La_{0.7}Sr_{0.3})_{0.95}MnO_3$ (LSM) and $(La_{0.7}Sr_{0.3})_{0.95}CoO_3$ (LSCo) for the cathode and the current-collecting layer, respectively, were synthesized via a modified glycine-nitrate-process. To improve the cathode performance and to prevent any interfacial reaction between the LSCo current-collecting layer and the YSZ electrolyte, a bi-layered cathode consisting of LSM/YSZ (60:40 wt.%) and LSM was applied before the current-collecting layer. The bi-layered cathode and the additional LSCo layer were also screen-printed on to the sintered anode–electrolyte substrate and were then co-fired at 1150 °C in air for 3 h. A photograph of the final 10 cm × 10 cm unit cells of 1 mm thickness is shown in Fig. 1.

Photographs of the sealing gasket and the interconnector for the SOFC stacks are shown in Fig. 2. For the planar SOFC stack, designs for the sealing and the interconnect are very important to ensure proper fuel and oxidant supply through the gas flow paths. In fact, there must be no leakage or build-up of gas pressure as both these factors can deteriorate both the performance and the efficiency of SOFCs during power generation. In general, glass-based materials are highly attractive for sealing purposes because of their structural deformability for gas tightness at high temperatures. Unfortunately, however, serious technical problems with glass-based sealants in terms of chemical and thermo-mechanical stability are still to be solved.

In this study, a unique compression-seal gasket design (Fig. 2(a)) has been developed. This was based on a glass and ceramic composite and showed extremely good sealing capability between neighboring components, i.e., YSZ electrolyte and inconnel-based alloys, in a general operating temperature range

Fig. 1. Photograph of anode-supported 10 cm × 10 cm unit cells.

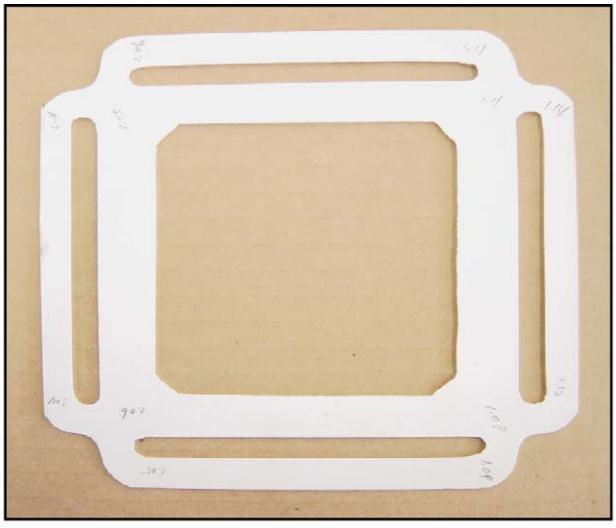

(a)

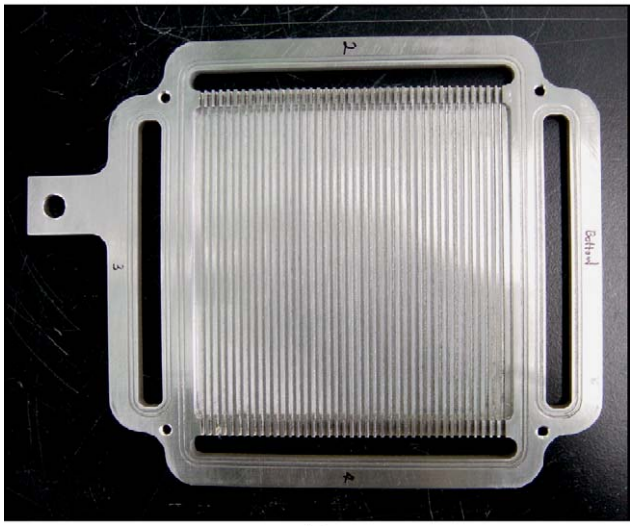

(b)

Fig. 2. Photographs of SOFC stack components: (a) sealing gaskets; (b) interconnector.

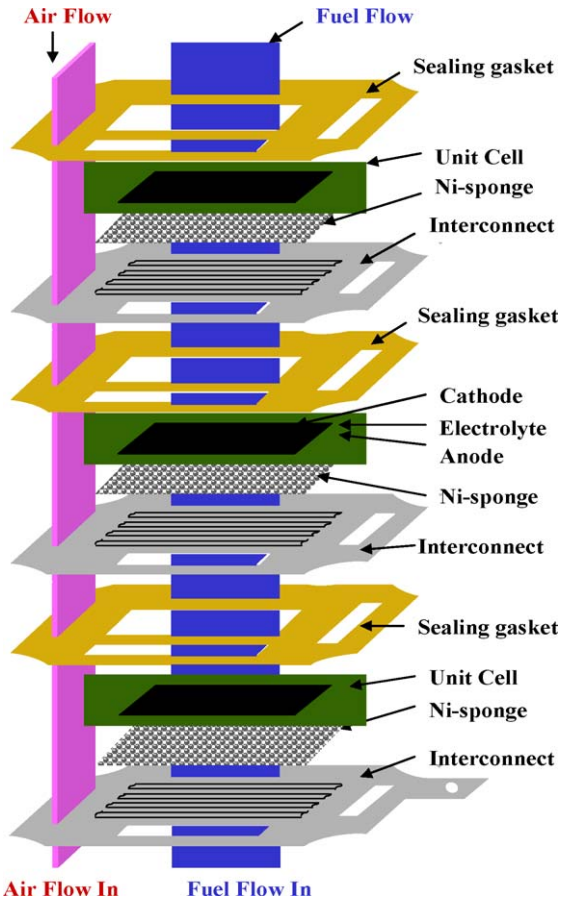

Fig. 3. Schematic diagram of planar SOFC stack based on anode-supported 10 cm × 10 cm unit cells.

of 700–800 °C. Moreover, this gasket type sealant could effectively reduce the thermal stresses between the stack components, so that rapid thermal cycling of the stack could become possible.

A commercial inconnel-based alloy was employed as a metal interconnect. This was chosen on an account of its rather good oxidation resistive characteristics even though it is not an entirely suitable material due to the great difference in thermal expansion coefficient from other stack components. The final outer shape of the inconnel-based interconnector with an internal gas manifold design is shown in Fig. 2(b).

A schematic diagram of the structure of the planar SOFC stacks developed in our laboratory is given in Fig. 3. Each stack segment consists of a ceramic-based 10 cm × 10 cm unit cell, a glass-based sealing gasket, and metallic interconnects. The gas flow channels of the interconnector were designed to induce a cross-flowing of fuel and oxidant gas. Considering the difference in the total flow rate between the fuel (H_2) and the oxidant (air) gas, the metallic interconnector (~5 mm thickness) was fabricated to have asymmetric cathode and anode gas manifolds with different areas. Porous Ni sponge was used as a current-collector and was inserted between the anode and the interconnector to achieve better electrical contact. A gasket-type compression sealant was applied to ensure gas tightness and to relieve the thermal stresses caused by mismatches of the thermal expansion coefficient between individual components of the SOFC stack during operation.

The current–voltage and current–power characteristics of the unit cell and short stacks were measured with a SOFC test station (Toyo, SAT890-100W) in a temperature range of 600–800 °C. Air was used as the oxidant and moisturized hydrogen (H_2 + 3% H_2O) as the fuel. For electrochemical characterization, a current-interruption technique was used to measure the ohmic loss (IR-drop) of the cells and an ac impedance measurement was used to evaluate the electrodic polarization.

3. Results and discussion

According to our previous investigations [7–9] on the electrode microstructure and its related physical properties, proper manipulation of the processing variables involved in electrode fabrication is essential to obtain optimum performance from the unit cell. In particular, the electrical and/or electrochemical properties of the electrode, which determine the ohmic and diffusional polarization losses in the unit cell, are normally tailored for the appropriate connection of the electrical and the gas diffusion paths. Based on these investigations, the fabrication technique was extended to produce a unit cell of larger area (10 cm × 10 cm) with a controlled electrode microstructure. The power-generating characteristics of this cell were then evaluated.

A scanning election micrograph of the cross-section of a 10 cm × 10 cm unit cell with a current-collecting layer is shown in Fig. 4. The unit cell is comprised of six different layers that include a single functional layer for the cathode and the anode sides, respectively. The thickness of the dense electrolyte layer is was about 8 μm and the overall cathode thickness is around 50 μm.

The power-generating curves of 10 cm × 10 cm (effective area 81 cm^2) anode-supported cells with an LSCo current-collecting layer are presented in Fig. 5. The cell was operated under the conditions of hydrogen with 3% H_2O as a fuel and air as an oxidant. A fuel utilization of 60% was determined from the criterion of ~0.7 V at 750 °C. The airflow was fixed as twice the stoichiometric amount ('2 stoichs'). The open-circuit voltage of the cell is in the range of 1.15–1.20 V for all temperature conditions. The power density of the cell is over 0.5 W cm^{-2} at

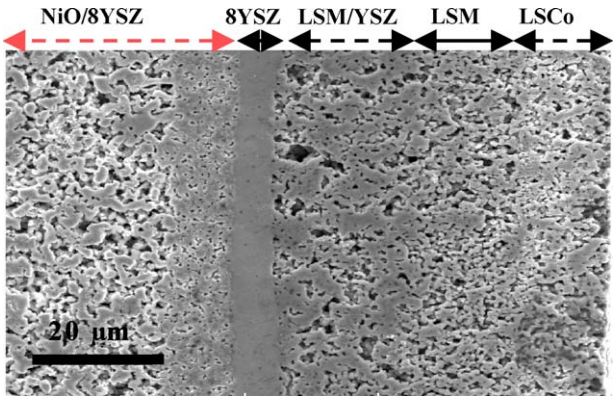

Fig. 4. Cross-sectional view of 10 × 10 unit cell with LSCo current-collecting layer.

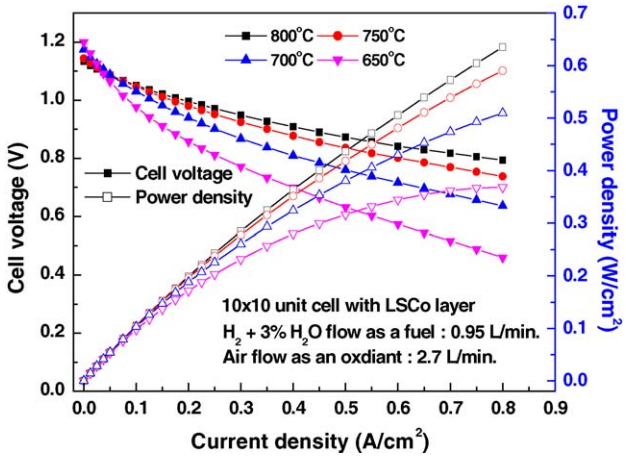

Fig. 5. Power-generating characteristics of 10 cm × 10 cm unit cell with LSCo layer at various operating temperatures (gas flow conditions of fuel and air are 60 and 160 L h^{-1}, respectively).

0.8 V at 750 °C. Furthermore, the cell area specific resistance (ASR) from current–voltage characteristics and the ohmic ASR from the dc interruption technique are about 0.362 Ω cm^2 (at 0.8 A cm^{-2}) and 0.174 Ω cm^2 at 750 °C, respectively.

The current–voltage and current–power characteristics of the 3-cell stack at various operating temperatures (700–900 °C) are shown in Fig. 6. The 3-cell stack was operated under similar operating conditions to that of the unit cell, i.e., $H_2 + 3\%$ H_2O was used as a fuel and air was used as an oxidant. The fuel utilization condition of 60% for each unit cell was also determined from the criterion of ~0.7 V at 800 °C and the airflow was fixed at 2 stoichs. As shown in Fig. 6, the open-circuit voltages (OCV) of the 3-cell stack are in a range from 3.41 to 3.48 V. This indicates that the OCV of each unit cell is about 1.14 V at 750 °C, which is comparable with that from unit cell test. The OCV value for the stack is almost equal to the theoretical value, which suggests that all the stack components are working properly without gas leakage with dense electrolyte, optimum electrical potential through the cells and tight stack housing.

A power density of over 0.43 W cm^{-2} at a stack voltage of 2.1 V (0.7 V per cell) was achieved at 750 °C and a total output power of about 100 W was obtained at 750 °C. Furthermore, under the operating conditions of 380 L h^{-1} airflow and 140 L h^{-1} fuel flow at 750 °C, a power output of 37 W per cell was attained with an electrochemical efficiency of 61% and a fuel utilization of 50%. By comparing the current–voltage characteristics in Figs. 5 and 6, the power density of 0.43 W cm^{-2}

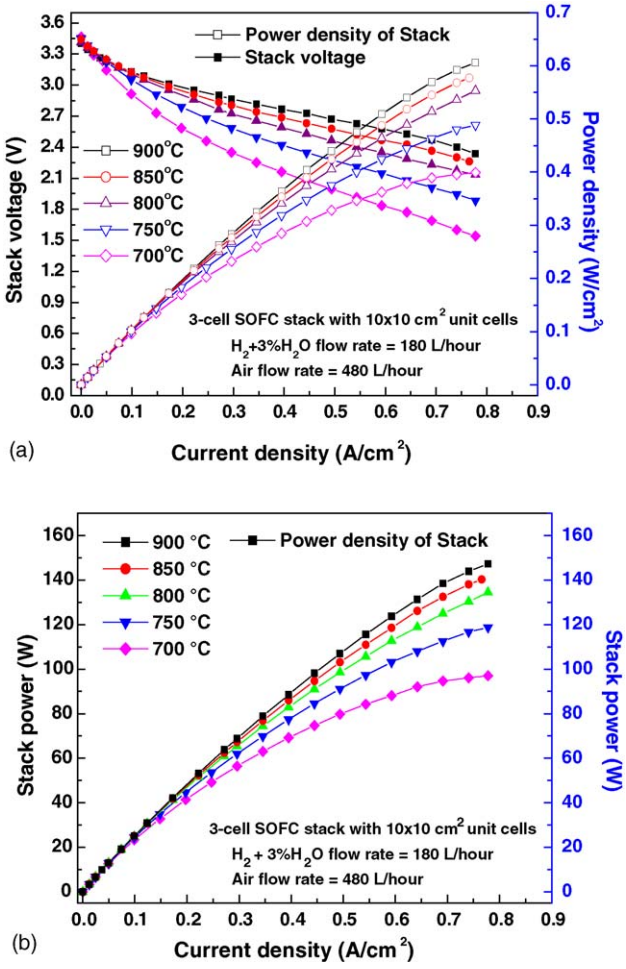

Fig. 6. Power-generating characteristics of 3-cell short stack with 10 cm × 10 cm unit cells at various operating temperatures (a) power density; (b) stack power plot (gas flow conditions of fuel and air are 140 and 380 L h^{-1}, respectively).

at 0.7 V per cell from the 3-cell stack is seen to be much lower than that from a unit cell under the same operation condition. The difference in power density between the stack and the unit cell can be attributed either to a change in ohmic ASR or to a change in polarization ASR.

The overall cell ASR and ohmic ASR values of a unit cell and a 3-cell stack are summarized in Table 1. The cell and ohmic ASR of the stack are around 0.667 and 0.265 Ω cm^2 per unit cell at 750 °C, respectively. Given that the cell and ohmic ASR from unit cell test are 0.506 and 0.174 Ω cm^2, a major portion of performance deterioration can be ascribed due to an increase in

Table 1
Area specific resistance (ASR) of a unit cell and a 3-cell stack measured at various temperatures (via current interruption measurements)

ASR\temperature (°C)	Unit cell		3-Cell stack	
	Ohmic ASR (Ω cm^2)	Cell ASR at 0.8 A cm^{-2} (Ω cm^2)	Average ohmic ASR (Ω cm^2 pre cell)	Average stack ASR at 0.8 A cm^{-2} (Ω cm^2 per cell)
700	0.239	0.643	0.369	0.823
750	0.174	0.506	0.265	0.667
800	0.126	0.401	0.189	0.563
850	0.093	0.313	0.162	0.499

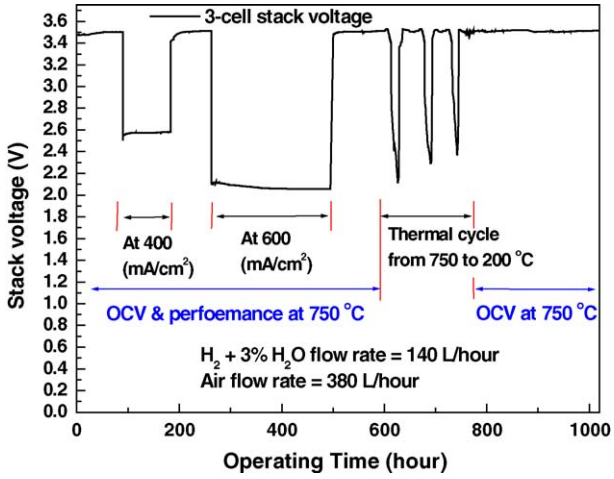

Fig. 7. Long-term stability and thermal cycling capability of 3-cell stack at 750 °C.

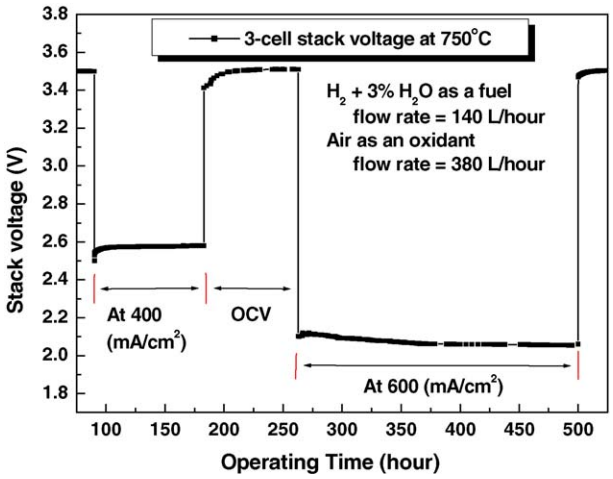

Fig. 8. 3-Cell short stack test under constant load conditions of 400 and 600 mA cm^{-2} at 750 °C.

ohmic ASR rather than in polarization ASR. This demonstrates that some scale-up problems had definitely occurred during the multi-cell stacking.

Such a scale-up problem is suspected to arise mainly from deterioration of the electrical contact between a cathode and an interconnect. In this study, a bare inconnel metal was used without any surface modification, such as an oxidation resistive coating or a highly conductive coating. Hence, a rather high resistive surface layer can be formed in oxidative atmosphere during the high temperature operation even though the interconnect has a relatively high resistance to oxidation. Moreover, the cathode layer can be easily damaged due to the much higher thermal expansion coefficient of the inconnel alloy, which might become another source of contact problem. Such contact problems at the cathode|interconnect interface can degrade not only the power-generating characteristics but also the long-term stability of the stack.

The durability and thermal cycle stability of the stack are shown in Fig. 7. The initial stack OCV gradually increases and stabilizes. To check the durability of the stack under special load operations, it was operated under loads of 400 and 600 mA cm^{-2}. During the first operation at 400 mA cm^{-2} between 90 and 190 h, the corresponding stack voltage gradually increases, as shown in Fig. 8. According to the current interruption test of the stack, this behaviour results from a decrease in the ohmic ASR of the stack from 0.281 to 0.265 Ω cm^2 per cell, which is nearly 80% of the total decrease in the stack ASR during this period (i.e., from 0.729 to 0.667 Ω cm^2 per cell at 0.8 A cm^{-2}). From these results, it can be concluded that the contact resistance between the electrode and the interconnect and/or the interface resistance between the electrode and the electrolyte can be improved by the current flowing during this initial period of the durability test. A similar observation has also been reported by Tsukuda and Yamashita [10].

After the first load test was stopped at 100 h, the stack voltage recovered rapidly to the initial OCV. As shown in Fig. 8, however, the second load test, under conditions of 600 mA cm^{-2} at the time interval of 260–500 h, showed a decrease in stack voltage. This observation can be attributed to an increase in the average stack ASR from 0.667 to 0.731 Ω cm^2 per cell (at 0.8 A cm^{-2}). From the impedance measurements and the current interruption test of the stack, it is concluded that an increase in stack ASR originates not only from an increase in ohmic resistance but also from an increase in electrode polarization. The probable causes of such performance degradation are as follows: (i) ageing of electrolyte at high temperatures; (ii) loss of Ni connectivity in the anode due to coarsening of Ni-particles and an increased vapour pressure of volatile Ni species (such as $Ni(OH)_2$) with increasing water; (iii) the formation of pores and a second phase at the electrode and electrolyte interface due to unwanted material transport under the current loading condition; (iv) decrease of electrochemical reaction sites due to the microstructural evolution of the electrode during operation; (v) deterioration of interfacial contact between the cathode and the interconnect, as described in previous work [11–16].

According to the impedance measurements and current interruption test of the stack, the average stack ASR changes from 0.667 to 0.781 Ω cm^2 per cell at 0.8 A cm^{-2} whereas the ohmic ASR changes from 0.265 to 0.274 Ω cm^2 per cell at 0.8 A cm^{-2}, which indicates that the electrode polarization loss is the main contributor to performance degradation. Thus, it can be tentatively concluded that the main cause of performance degradation during the second load test is electrode degradation rather than a contact problem, though specific details cannot be provided here. At present, it can be only anticipated that the contact problem is not the major concern under the constant-load test conditions. Nonetheless, more thorough investigations of the microstructural evolution in the electrode and electrode|interconnect interface are now underway and a more detailed explanation will be presented in future papers.

Three thermal cycling tests were performed at the time interval of 600 and 780 h. For each cycling test, the stack temperature was lowered from 750 to 200 °C and then increased again to 750 °C at a heating rate of more than 10 °C min^{-1}. As shown in Fig. 7, the stack OCV does not change significantly, whereas the stack ASR increases from 0.731 to 0.780 Ω cm^2 per cell (at

0.8 A cm^{-2}) after thermal cycling. From the impedance measurements and the current interruption test of the stack, it is found that stack performance is due mainly to an increase of ohmic resistance, especially related to the contact resistance between the interconnect and the electrode. Nevertheless, from the results of the durability and thermal-cycling tests, it was demonstrated that all the stack components (except the interconnect) were working properly for more than 1000 h at 750 °C, even under severe operation conditions. In particular, the sealing material proved durable against thermal cycling and was very effective for reducing the thermal stress between the stack components. Further post-mortem characterization of the stack to verify this interpretation will be addressed in a future paper.

4. Conclusion

Planar-type stacks with an internal gas manifold and a cross-flow type design are assembled from 10 cm × 10 cm anode-supported cells, inconnel-based interconnects and glass-based compression-seal gaskets. According to the performance evaluation of a 3-cell stack, 100 W is obtained under an electrical efficiency of 61% and a fuel utilization of 50% at 750 °C. The durability and reliability of the short stack are verified by long-term operations under various load conditions and additional thermal cycling tests.

Acknowledgements

This work was supported by the Core Technology Development Program for Fuel Cells, the NRL Program of the Ministry of Science and Technology of Korea and the Korea Institute of Science and Technology Evaluation and Planning.

References

[1] N.Q. Minh, J. Am. Ceram. Soc. 76 (1993) 563.
[2] N.Q. Minh, T. Takahashi, Science and Technology of Ceramic Fuel Cells, Elsevier, Amsterdam, 1995 (Chapters 1–5).
[3] S.C. Singhal, K. Kendall, in: S.C. Singhal, K. Kendall (Eds.), High Temperature Solid Oxide Fuel Cells, Elsevier, UK, 2003, p. 1.
[4] J.-H. Lee, H. Moon, H.-W. Lee, J. Kim, J.-D. Kim, K.-H. Yoon, Solid State Ionics 148 (2002) 15.
[5] D.-S. Lee, J.-H. Lee, J. Kim, H.-W. Lee, H.-S. Song, Solid State Ionics 166 (2004) 13.
[6] H. Wendt, O. Bijhme, F.U. Leidich, in: D. Shores, H. Maru, I. Uchiden, J.R. Selman (Eds.), Carbonate Fuel Cell Technology, The Electrochemical Society, 1993, p. 485.
[7] J.-H. Lee, J.-W. Heo, D.-S. Lee, J. Kim, G.-H. Kim, H.-W. Lee, H.-S. Song, J.-H. Moon, Solid State Ionics 158 (2003) 225.
[8] K.-R. Lee, S.H. Choi, J. Kim, H.-W. Lee, J.-H. Lee, J. Power Sources 140 (2005) 226.
[9] H.Y. Jung, W.-S. Kim, S.-H. Choi, H.-C. Kim, J. Kim, H.-W. Lee, J.-H. Lee, J. Power Sources 155 (2006) 145–151.
[10] H. Tsukuda, A. Yamashita, in: U. Bossel (Ed.), First European Solid Oxide Fuel Cell Forum, Switzerland, 1994, p. 715.
[11] M.J. Jorgensen, P. Holtappels, C.C. Appel, J. Appl. Electrochem. 30 (2000) 413.
[12] T. Norby, P.A. Osborg, H. Raeder, in: U. Bossel (Ed.), First European Solid Oxide Fuel Cell Forum, Switzerland, 1994, p. 671.
[13] A.C. Muller, A. Weber, E. Ivers-Tiffee, in: M. Mogensen (Ed.), Sixth European Solid Oxide Fuel Cell Forum, Switzerland, 2004, p. 1231.
[14] H.-I. Yoo, K.-C. Lee, J. Electrochem. Soc. 145 (1998) 4243.
[15] J.-O. Hong, H.-I. Yoo, Solid State Ionics 113–115 (1998) 265.
[16] D. Monceau, M. Filal, M. Tebtoub, C. Petot, G. Petot-Ervas, Solid State Ionics 73 (1994) 221.